JACS
JOURNAL OF THE AMERICAN CHEMICAL SOCIETY

Article

pubs.acs.org/JACS

Acid-Active Cell-Penetrating Peptides for in Vivo Tumor-Targeted Drug Delivery

Erlei Jin,[†,∥] Bo Zhang,[†,∥] Xuanrong Sun,[‡] Zhuxian Zhou,[†] Xinpeng Ma,[†] Qihang Sun,[†] Jianbin Tang,[‡] Youqing Shen,*[,‡] Edward Van Kirk,[§] William J. Murdoch,[§] and Maciej Radosz[†]

[‡]Center for Bionanoengineering and State Key Laboratory for Chemical Engineering, Department of Chemical and Biological Engineering, Zhejiang University, Hangzhou, China 310027

[†]Department of Chemical and Petroleum Engineering and [§]Department of Animal Science, University of Wyoming, Laramie, Wyoming 82071, United States

Supporting Information

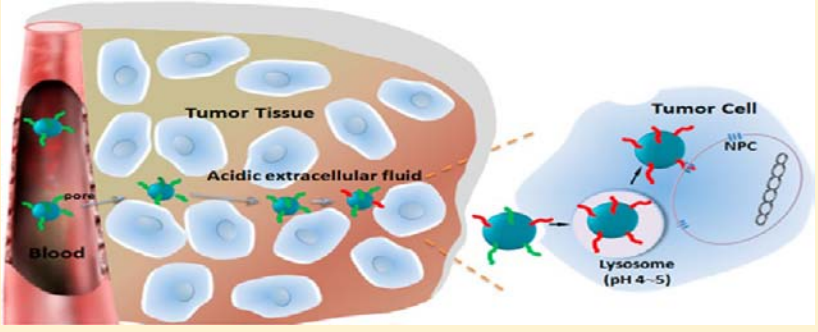

ABSTRACT: Cell-penetrating peptides (CPPs) such as transactivator of transcription (TAT) peptide have long been explored for promoting in vitro cell penetration and nuclear targeting of various cargos, but their positive charges cause strong nonspecific interactions, making them inapplicable for many in vivo applications. In this work, we used TAT to demonstrate a molecular modification approach for inhibiting nonspecific interactions of CPPs in the bloodstream while reactivating their functions in the targeted tissues or cells. The TAT lysine residues' amines were amidized to succinyl amides ([a]TAT), completely inhibiting TAT's nonspecific interactions in the blood compartment; once in the acidic tumor interstitium or internalized into cell endo/lysosomes, the succinyl amides in the [a]TAT were quickly hydrolyzed, fully restoring TAT's functions. Thus, [a]TAT-functionalized poly(ethylene glycol)-*block*-poly(ε-caprolactone) micelles achieved long circulation in the blood compartment and efficiently accumulated and delivered doxorubicin to tumor tissues, giving rise to high antitumor activity and low cardiotoxicity. This amidization strategy effectively and easily enables in vivo applications of CPPs.

Cell-penetrating peptides (CPPs), highly cationic peptides usually rich in arginine and lysine amino acids, are characterized by their ability to translocate quickly into almost any live cells.[1,2] Some sequences, such as the protein transduction domain from HIV transactivator of transcription (TAT) protein (GRKKRRQRRRPPQ),[3] can be recognized by the nuclear pore complexes (NPCs)[4] and thus can actively transport proteins,[5] DNA,[6,7] nanoparticles,[2,8] and other cargos from the cytosol into cell nuclei. Therefore, CPPs have been used as exceptionally efficient "locomotives" for intracellular and nuclear delivery of various cargos ranging from such small molecules as anticancer drugs[9] to macromolecules as large full-length proteins and peptides[10] and even nanoparticles.[11,12]

However, given the tremendous application potential demonstrated by numerous in vitro studies,[2,13] CPPs are inapplicable for many in vivo uses because of their inherent nonspecificity caused by their cationic nature. For instance, β-galactosidase-TAT-fused protein injected intraperitoneally into mice was found to be distributed in practically all tissues.[14] Once intravenously (i.v.) administered, CPPs activate reticuloendothelial system recognition; thus, they are rapidly cleared from circulation and readily penetrate into most organs.[15]

Shielding of the cationic charges of CPPs with polyanions is used to suppress their nonspecific interactions. For instance, a CPP was fused with an anionic peptide via a cleavable linker to mask its cell-penetrating functions and also its nonspecific interactions by intramolecular electrostatic interactions. Once in the target tissues such as tumors, proteolysis of the linker facilitated the disassociation of the two domains, activating the CPP's functions.[16,17] However, a recent report revealed that the activation was tumor-independent and most likely occurred in the vasculature.[16] Sethuraman and Bae proposed acid-sensitive deshielding using a synthetic pH-responsive polymer that is negatively charged under neutral conditions but becomes neutral in an acidic environment. Thus, the polymer formed complexes

Received: November 14, 2012
Published: December 19, 2012

   dx.doi.org/10.1021/ja311180x | J. Am. Chem. Soc. 2013, 135, 933−940

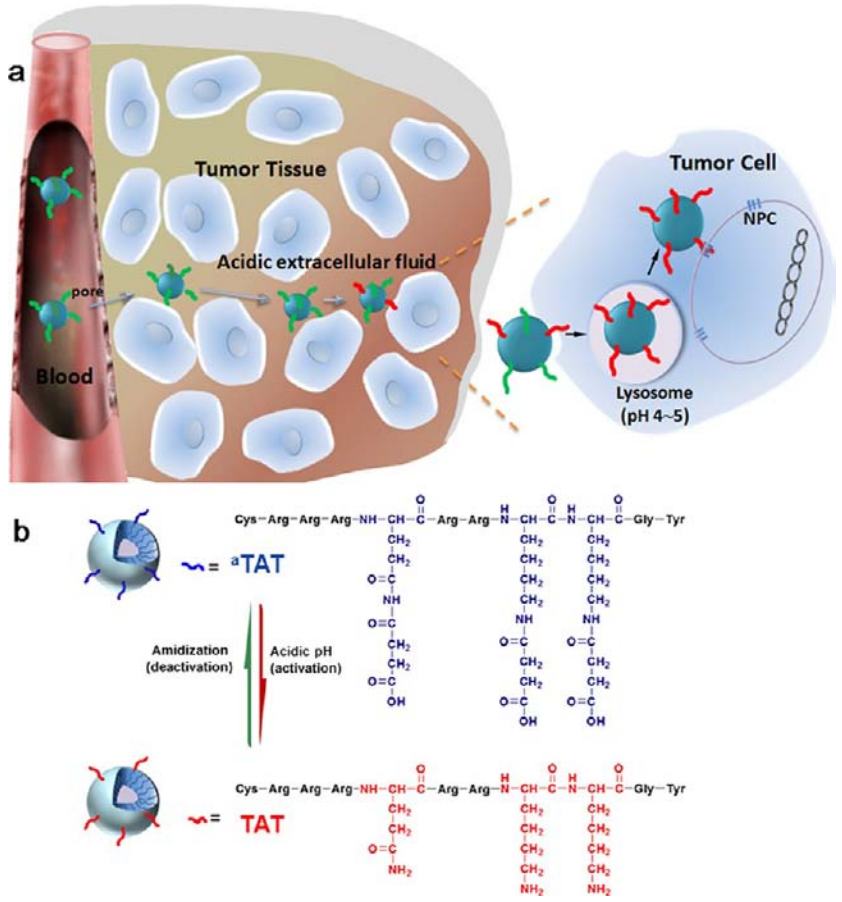

Figure 1. (a) Illustration of the use of TAT as an example of a cell-penetrating peptide (CPP) to demonstrate the concept of deactivation of a CPP in the blood compartment and its activation in the tumor interstitium or cells for in vivo tumor-targeted drug delivery. The amines of the lysine residues of a CPP are amidized to inhibit its nonspecific interactions in the blood compartment without affecting the nanocarriers' stealth properties. Once the nanocarrier extravasates into tumor tissue through highly permeable blood vessels via the EPR effect, these amides are hydrolyzed, regenerating the pristine functioning CPP in the acidic tumor extracellular fluids (pH < 7) for fast cellular uptake or in acidic endo/lysosomes for fast endo/lysosomal escape and nuclear targeting. (b) Amidization of TAT's primary amines to succinyl amides and their acid-triggered hydrolysis.

at a neutral pH but fell off the TAT at acidic pH.[18] The main concern with this method is the in vivo stability of the complexation because a short TAT peptide contains a limited number of positive charges; therefore, its electrostatic interaction is very weak. As a reference, even the complexes of TAT with large anionic macromolecules such as DNA dissociate quickly in the presence of serum proteins.[19] Bae and co-workers also proposed a "pop-up" method in which TAT was anchored onto the micelle surface via pH-sensitive polyhistidine (polyHis).[20] PolyHis was water-insoluble at pH 7.4, and thus, the TAT was buried in the hydrophilic PEG corona; at acidic pH, the polyHis became water-soluble, exposing the TAT on the micelle surface for binding. This method may not be applicable for nuclear delivery, however: once in the cytoplasm, whose pH is around 7.4, the TAT moieties would again be buried in the PEG corona.

Herein we demonstrate a molecular modification strategy for in vivo CPP applications. Almost all CPPs contain lysine residues; their primary amines are the main cause of the nonspecific interactions, but they also play a key role in their membrane transduction and nuclear localization functions.[21] Some β-carboxylic amides are stable at neutral pH but quickly hydrolyze at acidic pH to regenerate the corresponding amines.[22] We thus hypothesized that amidizing the lysine residue amines to acid-labile amides would inactivate the CPPs, inhibiting their nonspecific interactions in the bloodstream. Once in the acidic tumor interstitium (pH < 7[23]) or cell endo/lysosomes (pH 4–5), the acid-labile amides would be hydrolyzed, activating the CPPs and exposing their functions (Figure 1a). This strategy would enable CPPs to be used in various in vivo applications, particularly in delivery systems.

The key question of this hypothesis is whether amidization of lysine residue amines is sufficient to inactivate the CPPs because they also contain arginine residues, whose cationic guanidinyl groups cannot be amidized easily. Herein we selected an arginine-rich TAT peptide containing two lysine residues and five arginine residues to test our hypothesis (Figure 1b). We tethered TAT and its amidized product, denoted as ^{a}TAT, to the corona of poly(ethylene glycol)-*block*-poly(ε-caprolactone) (PEG-PCL) micelles and compared the in vitro and in vivo properties of the resulting functionalized micelles (TAT-PEG-PCL and ^{a}TAT-PEG-PCL, respectively). In contrast to the fast clearance of TAT-functionalized micelles, the ^{a}TAT-PEG-PCL micelles had no nonspecific interactions with the blood components and thus circulated in the bloodstream the same as nonfunctionalized PEG-PCL micelles. More importantly, ^{a}TAT-PEG-PCL preferentially accumulated in tumor tissues, where the ^{a}TAT was regenerated to TAT in the tumor's acidic extracellular interstitium and lysosomes; the regained functions of TAT led to high in vivo therapeutic efficacy.

dx.doi.org/10.1021/ja311180x | J. Am. Chem. Soc. 2013, 135, 933–940

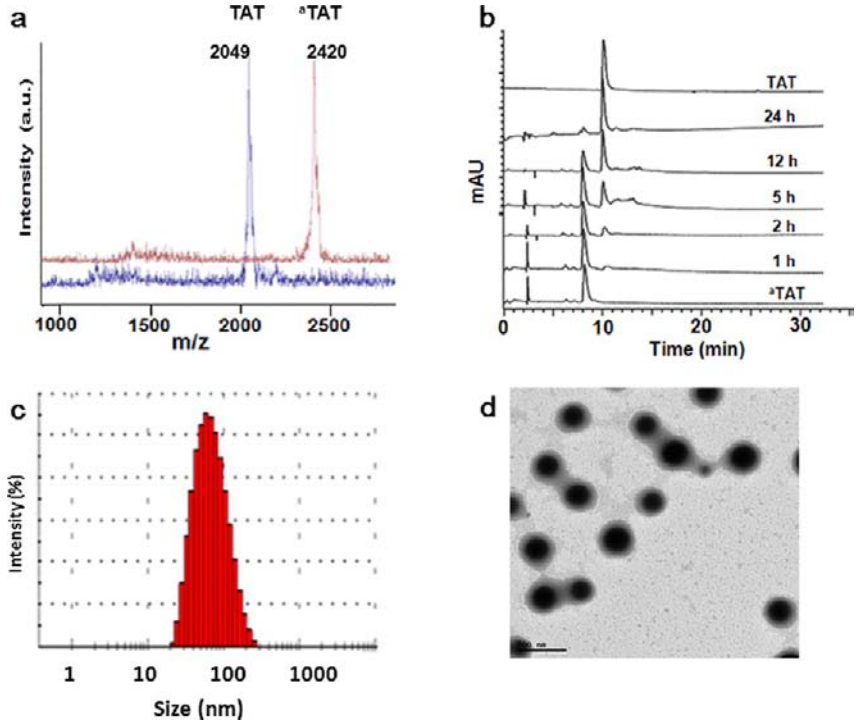

Figure 2. (a) Molecular weights of TAT before and after amidization (^{a}TAT) as determined by MALDI-TOF MS. The molecular weight difference corresponds to three $-OCCH_2CH_2COONa$ groups. (b) HPLC traces of ^{a}TAT after incubation at pH 5.0 and 37 °C for different times. (c) Size distribution of ^{a}TAT-functionalized poly(ethylene glycol)-*block*-poly(ε-caprolactone) micelles (^{a}TAT-PEG-PCL) loaded with 13.6 wt % doxorubicin (DOX) as determined by dynamic light scattering. (d) Morphology of ^{a}TAT-PEG-PCL as observed using transmission electron microscopy (scale bar = 200 nm). The micelles were stained with 2% phosphotungstic acid.

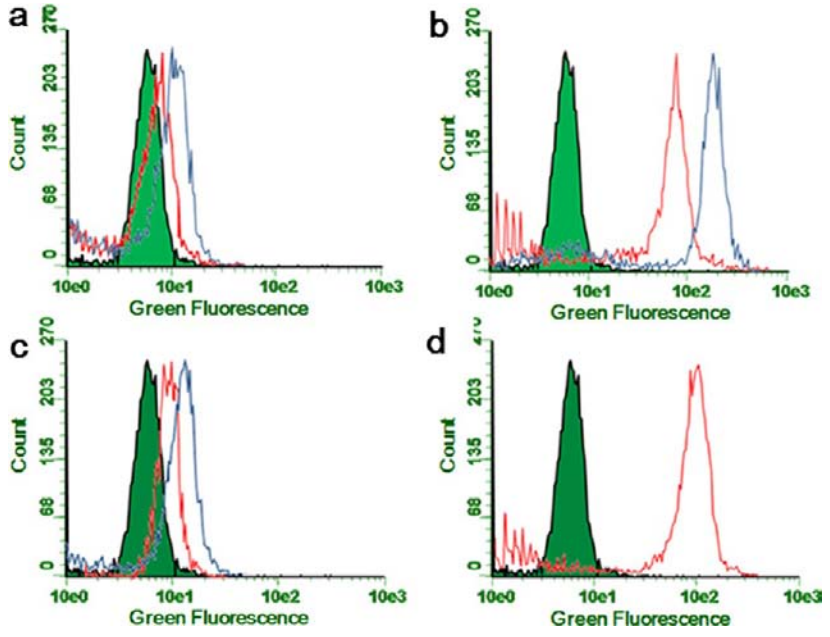

Figure 3. DOX-positive cell populations measured by flow cytometry of SKOV-3 ovarian cancer cells cultured with (a) PEG-PCL/DOX for 1 h (red curve, 3.2%) and 5 h (blue, 15.3%), (b) TAT-PEG-PCL/DOX for 1 h (red curve, 58.6%) and 5 h (blue, 73.7%), (c) ^{a}TAT-PEG-PCL/DOX for 1 h (red curve, 7.8%) and 5 h (blue, 21.2%), and (d) ^{a}TAT-PEG-PCL/DOX (preincubated at pH 5.0 for 8 h) for 5 h (red curve, 64.2%). All of the populations are referenced to the same control cells (green-shaded peaks, 0.8%). The DOX dose was 1 μg/mL.

RESULTS AND DISCUSSION

TAT Amidization and Micelle Functionalization. The TAT lysine residue amines were first amidized using anhydrides, including 4-cyclohexene-1,2-dicarboxylic anhydride, 2,3-dimethylmaleic anhydride, and 2,2,3,3-tetramethylsuccinic anhydride used in our and other reports,[24] but the amides from those anhydrides hydrolyzed very quickly, even at neutral pH (data not shown). We finally found that amidization using an excess of succinyl chloride produced the expected product (Figure 1b). As determined by matrix-assisted laser desorption ionization time of

dx.doi.org/10.1021/ja311180x | J. Am. Chem. Soc. 2013, 135, 933−940

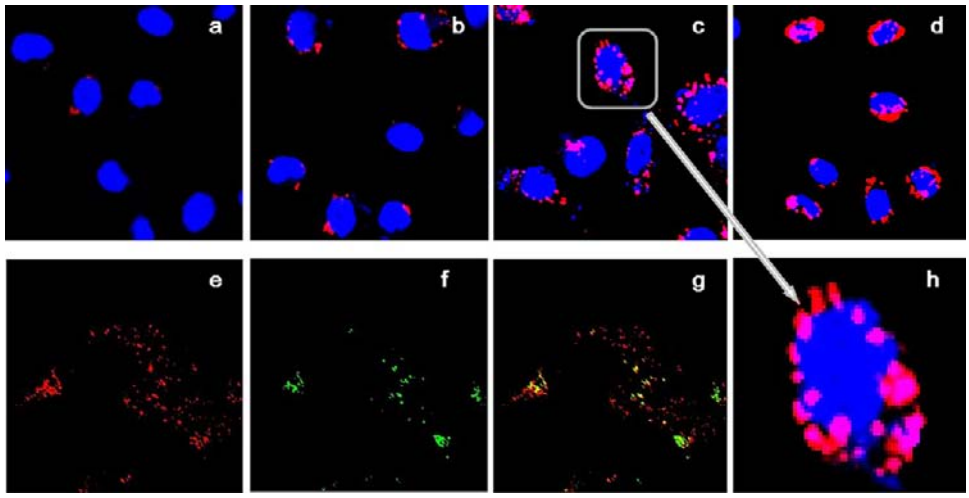

Figure 4. Cellular uptake and intracellular localization of ^{a}TAT-PEG-PCL/nile red micelles observed by confocal laser scanning microscopy. SKOV-3 ovarian cancer cells were cultured with ^{a}TAT-PEG-PCL/nile red at a nile red dose of 1 μg/mL for (a) 1, (b) 5, (c) 12, and (d) 24 h. An amplification of one cell in (c) is shown in (h). Lysosomal colocalization of ^{a}TAT-PEG-PCL/nile red in the cells after incubation for 5 h at 37 °C was observed by confocal microscopy through (e) the nile red channel and (f) the LysoTracker green channel. The overlap of the images in (e) and (f) is shown in (g). The nuclei were stained with DRAQ5 (blue). Nile red-loaded micelles appear in red and lysosomes stained with LysoTracker in green. The original magnification is 63×. The images of the PEG-PCL and TAT-PEG-PCL controls are shown in Figure S5 in the Supporting Information.

flight mass spectrometry (MALDI-TOF MS) (Figure 2a), the molecular weight difference between ^{a}TAT and TAT was 371, corresponding to three succinyl residues with three sodium ions, suggesting that in addition to the amidization of the two lysine residue amines to the succinyl amides, the glutamine amide was also amidized to give the succinyl imide,[25] while the guanidinyl groups were not affected (Figure 1b).

The stability of ^{a}TAT was evaluated by monitoring its hydrolysis at pH 5.0 using HPLC (Figure 2b). Some TAT was regenerated after incubation for 2 h, and almost all of the ^{a}TAT was converted to pristine TAT in 24 h. This was very surprising because previous work by others and us found that the succinyl amides of the primary amines in polylysine (PLL) and poly(amidoamine) dendrimers were barely hydrolyzable at pH 5.0 or even lower pH.[24,26] We postulated that the greater hydrolysis of the succinyl amides in ^{a}TAT might be due to the catalysis of the adjacent guanidinyl groups. To confirm this, we guanidinated 50% of the primary amines in a PLL with a number-average molecular weight of 2 kDa and amidized the remaining primary amines to succinyl amides. Indeed, the succinyl amides in the guanidinated PLL were very stable at pH 7.4 but underwent fast hydrolysis at pH 5.0 (Figure S2 in the Supporting Information).

The synthesis and characterization of the TAT-functionalized PEG-PCL copolymers are detailed in the Supporting Information (see Figure S1). Micelles functionalized with TAT or ^{a}TAT were fabricated by dialysis of a mixture of PEG-PCL with TAT-PEG-PCL or ^{a}TAT-PEG-PCL. After optimizations, we found that 15 mol % TAT-PEG-PCL or ^{a}TAT-PEG-PCL in the micelles (i.e., ^{a}TAT-PEG-PCL/PEG-PCL = 15/85) was optimal for the following comparison of the micelle properties and was thus used in the following study. The micelles were encapsulated with either the hydrophobic dye DiR for tracing or the anticancer drug doxorubicin (DOX) for therapy. The ^{a}TAT-PEG-PCL micelles were about 70 nm in diameter in phosphate-buffered solution (PBS, pH 7.4), as measured by dynamic laser light scattering (Figure S3 in the Supporting Information). They grew to 75 nm in diameter after loading with 13.6 wt % DOX (Figure 2c,d) and 92 nm after loading with 14.3 wt % DiR (Figure S3). These sizes are known to be optimal for passive accumulation into tumor tissues via the enhanced permeation and retention (EPR) effect.[27]

Cellular Internalization and Intracellular Distribution. The cellular uptakes of the DOX-loaded micelles were compared by flow cytometry. PEG-PCL/DOX micelles entered SKOV-3 cells very slowly (Figure 3a). After 1 or 5 h culture with PEG-PCL/DOX micelles, only 3.2 or 15.3% of the cells, respectively, had a barely measurable DOX fluorescence. Of the cells cultured with TAT-PEG-PCL/DOX micelles, 58.6% after 1 h culture and 73.7% after 5 h culture had very strong DOX fluorescence, suggesting very quick cellular uptake of the TAT-functionalized micelles (Figure 3b). The cellular uptake of ^{a}TAT-PEG-PCL/DOX was very similar to that of PEG-PCL/DOX and significantly slower than that of TAT-PEG-PCL/DOX (Figure 3c). This indicates that ^{a}TAT could not interact with the cells as pristine TAT did. However, once ^{a}TAT-PEG-PCL micelles were first incubated at pH 5.0 for 8 h, their cellular uptake became as fast as that of TAT-PEG-PCL/DOX (Figure 3d), suggesting the recovery of fully functioning TAT moieties on the micelle surface.

The cellular uptake and subsequent intracellular distribution of the micelles were studied by confocal fluorescence microscopy. As the images of fixed cells have been shown to cause major artifacts in the intracellular localization of CPPs, we used live cells for fluorescence microscopy studies. Nile red rather than DOX was used here to trace the micelles because DOX itself efficiently concentrates in the nuclei but nile red does not. In agreement with the flow-cytometry results and other reports in the literature,[28] the cellular uptake of TAT-PEG-PCL/nile red was much faster than that of PEG-PCL/nile red; significantly, the micelles were found to be dotted on the nuclear membranes (Figure S4 in the Supporting Information). The cellular internalization of ^{a}TAT-PEG-PCL/nile red (Figure 4a,b) was very similar to that of PEG-PCL/nile red (Figure S4) at short incubation times. Few ^{a}TAT-PEG-PCL/nile red micelles were observed in the cells after incubation for 1 h, whereas more and more red dots were found in the cells when the culture time was prolonged to 12 or 24 h (Figure 4c,d). The internalized micelles

dx.doi.org/10.1021/ja311180x | J. Am. Chem. Soc. 2013, 135, 933−940

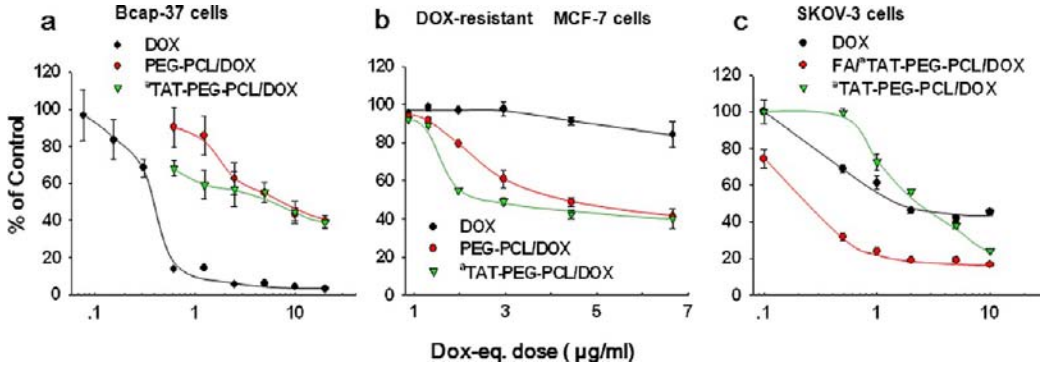

Figure 5. Cytotoxicities of DOX and DOX-loaded micelles toward (a) non-drug-resistant Bcap-37 breast cancer cells, (b) DOX-resistant MCF-7 breast cancer cells, and (c) folate-receptor-overexpressing SKOV-3 ovarian cancer cells. The cells were treated with DOX or DOX-loaded micelles for 24 h followed by 24 h postculture before analysis by MTT assay [n = 3, data expressed as average ± standard error (SE)]. SKOV-3 cells were cultured in folate-free medium for at least 2 weeks before the experiment.

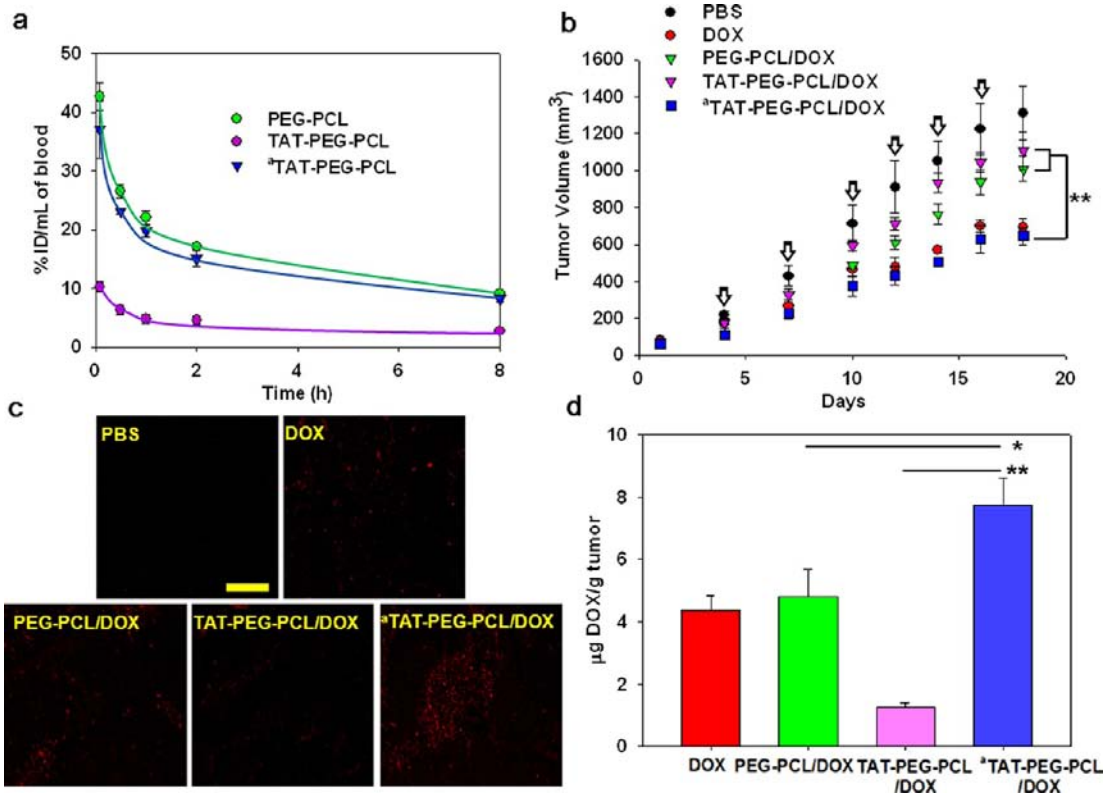

Figure 6. (a) Blood clearance of the micelles, (b) in vivo tumor inhibition of DOX and DOX-loaded micelles, and (c, d) their DOX accumulations in tumors (c) as observed by confocal microscopy or (d) as quantitated in terms of micrograms of DOX per gram of tumor tissue. (a) In the blood-clearance experiments, the micelles were loaded with 14.3 wt % DiR. The micelle content in the blood was expressed as percent of the injected dose (ID) per milliliter of blood (n = 3, data expressed as average ± SE). (b) In the tumor inhibition experiments, PBS or DOX was i.v. administered to Bcap-37-xenografted nude mice at an equivalent dose of 4 mg/kg every 2 or 3 days, as indicated by the arrows; each tumor was measured at the time of the injection, and its tumor volume was calculated (n = 5, data expressed as average ± SE, ** denotes $p < 0.01$). (c) At the end of the experiment, the tumors were dissected, fixed, and embedded in paraffin. The DOX accumulation in tumor sections was observed by confocal microscopy at the exact same settings. Scale bar =50 μm. (d) The DOX concentration was calculated from the DOX in the acidified isopropanol extraction solution of the homogenized tumor tissue (n = 3, data expressed as average ± SE, * denotes $p < 0.05$, ** denotes $p < 0.01$).

were found initially to be localized in the lysosomes, as evidenced by the yellow spots in the overlap image (Figure 4g) obtained from the images of the micelles (red, Figure 4e) and lysosomes (green, Figure 4f). This indicated that like the PEG-PCL micelles, [a]TAT-PEG-PCL nanoparticles were internalized via the endocytosis pathway into endo/lysosomes, where [a]TAT could hydrolyze and regenerate TAT. Indeed, after incubation for 5 h, many micelles were no longer located in the endo/lysosomes (red dots, Figure 4g), suggesting successful escape from the endo/lysosomes. Further, many [a]TAT-PEG-PCL micelles were found punctuated on the nuclear membranes (Figure 4c and the enlarged view of one cell in Figure 4h), particularly after 24 h. This phenomenon was very different from that of the PEG-PCL micelles, which remained trapped in the endo/lysosomes and were not associated with the cell nuclei even after long culture times,[29] but the same as the punctuated distribution of TAT-

dx.doi.org/10.1021/ja311180x | J. Am. Chem. Soc. 2013, 135, 933−940

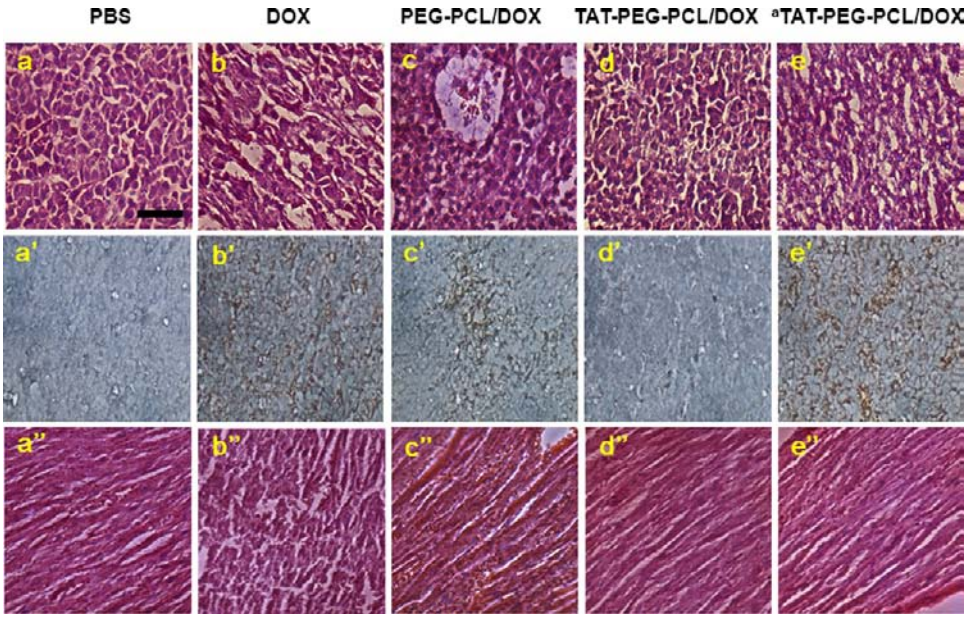

Figure 7. (a–e) H&E and (a′–e′) TUNEL staining of the tumor sections and (a″–e″) H&E staining of the heart sections of the mice after treatments. Tissue paraffin sections were 7 μm thick. In (a–e), the tumor sections were stained with hematoxylin/eosin (H&E) and examined by light microscopy. In (a′–e′), the TdT-mediated dUTP nick end labeling (TUNEL) assay was used to determine the apoptotic cells in situ in the dissected tumor tissue slides. Apoptotic cells were identified by positive TUNEL staining (brown) under light microscopy. In (a″–e″), the heart sections were stained with H&E and examined by light microscopy. Scale bar = 50 μm.

PEG-PCL/nile red on the nuclear membranes (Figure S4). These findings are in agreement with the TAT's function that can lead to fast escape of cargo from endo/lysosomes and its quick translocation to the perinuclear region and even nuclear localization.[12] TAT, as a nuclear localizing signal (NLS), can bind NPCs and carry small cargos into the nuclei. An NLS can ship particles with diameters of up to 39 nm through the nuclear pores.[30] Another recent study has shown that TAT-conjugated nanoparticles smaller than 50 nm could freely enter through NPCs, while large nanoparticles (>67 nm) could not.[31] Thus, comparison of the results in Figure 4c,d with those in Figure S5 confirmed that once internalized into a lysosome, the ^{a}TAT on the micelle was regenerated into TAT, which enabled the micelle to escape into the cytosol, traverse to the perinuclear region, and subsequently bind the NPCs. However, because of the large particle size (75 nm), these micelles could not be dragged into the nuclei but were docked on the nuclear pores.

The intracellular behavior of ^{a}TAT was further probed by comparing the cytotoxicities of DOX delivered by these micelles (Figure 5). DOX delivered by ^{a}TAT-PEG-PCL and PEG-PCL micelles exhibited very similar cytotoxicities toward non-drug-resistant Bcap-37 breast cancer cells that were much lower than the cytotoxicity of free DOX (Figure 5a). This occurred because free DOX could very quickly diffuse into the non-drug-resistant cells, inducing high cytotoxicity, whereas both ^{a}TAT-PEG-PCL and PEG-PCL micelles entered cells very slowly at similar rates (as shown in Figure 3) and thus slowly delivered DOX into the cells. However, free DOX at doses less than 8 μg/mL showed little cytotoxicity toward DOX-resistant MCF-7 cells (Figure 5b) because these cells could effectively reduce the intracellular DOX accumulation using their multidrug resistance mechanisms.[32] DOX loaded in micelles could bypass these mechanisms, and therefore, ^{a}TAT-PEG-PCL/DOX showed dose-dependent cytotoxicity with a half-maximal inhibitory concentration (IC_{50}) of 2 μg/mL, slightly better than that of PEG-PCL/DOX. To enhance the cellular uptake and elucidate the regeneration of TAT in endo/lysosomes, folic acid (FA) was introduced into the micelles as a targeting group. FA can bind folate receptors on cell membranes, triggering fast endocytosis into lysosomes.[33] (FA/^{a}TAT)-PEG-PCL micelles were fabricated from an 85/15/10 mixture of PEG-PCL, ^{a}TAT-PEG-PCL, and FA-PEG-PCL. The cytotoxicities of DOX delivered by ^{a}TAT-PEG-PCL and (FA/^{a}TAT)-PEG-PCL were compared using SKOV-3 ovarian cancer cells overexpressing folate receptors induced by culturing them with folate-free medium.[33] As shown in Figure 5c, (FA/^{a}TAT)-PEG-PCL/DOX had much higher cytotoxicity than ^{a}TAT-PEG-PCL/DOX and even free DOX, even though this cell line is not DOX-resistant. This comparison is in good agreement with the results discussed above: ^{a}TAT had no interaction with cells, and thus, ^{a}TAT-PEG-PCL micelles were internalized very slowly into endo/lysosomes; however, once inside the endo/lysosomes, ^{a}TAT was efficiently hydrolyzed into TAT, leading to fast lysosomal escape and nuclear localization, where DOX could exert its pharmaceutical actions.

In Vivo Stability and Tumor-Targeted Drug Delivery of Amidized TAT. The in vivo stability of ^{a}TAT was evaluated by monitoring the blood clearance of the corresponding micelles (Figure 6a). A near-IR fluorescence dye, DiR, was loaded in the micelles as a tracer since the excitation and emission wavelengths of DiR do not overlap with the autofluorescence of blood, allowing its concentration to be measured directly from the whole blood fluorescence. In agreement with other reports,[15] the i.v.-injected TAT-PEG-PCL micelles were rapidly cleared from the bloodstream: in as little as 1 h after the injection, the fluorescence of TAT-PEG-PCL/DiR in the blood was hardly detectable. In contrast, ^{a}TAT-PEG-PCL/DiR had a very slow clearance profile similar to that of PEG-PCL/DiR. These results indicated that ^{a}TAT indeed caused no nonspecific interactions with the blood component and that the succinyl amides in ^{a}TAT are very stable in blood.

dx.doi.org/10.1021/ja311180x | J. Am. Chem. Soc. 2013, 135, 933–940

The prolonged blood circulation time should enhance the possibility that the micelles extravasate from the tumor blood vessels into tumor tissues via the EPR effect.[27] The accumulation in tumor tissues and therapeutic efficacy of DOX delivered by the micelles were subsequently tested using a xenograft tumor model (Figure 6b). The tumor growth of mice administrated with ^{a}TAT-PEG-PCL/DOX was much slower than that of mice treated with TAT-PEG-PCL/DOX or PEG-PCL/DOX, and this difference became more significant ($p < 0.01$) after day 15. After the mice were sacrificed, the tumors were dissected and weighed, and the tumor-inhibition rate (TIR) of each group was calculated accordingly. A 47% TIR was achieved in the mice treated with ^{a}TAT-PEG-PCL/DOX, compared with TIRs of 29 and 18% for PEG-PCL/DOX and TAT-PEG-PCL/DOX, respectively (Figure S5 in the Supporting Information). Thus, compared with TAT-PEG-PCL/DOX and PEG/PCL/DOX, ^{a}TAT-PEG-PCL/DOX showed a significantly ($p < 0.05$) enhanced therapeutic efficacy. Further observation of the tumor sections by confocal microscopy at the excitation wavelength of DOX (Figure 6c) showed that there was more DOX in the tumors treated with ^{a}TAT-PEG-PCL/DOX than in the other tumors. Quantitation of DOX in the homogenized dissected tumors showed that ^{a}TAT-PEG-PCL/DOX-treated tumors had twice the DOX concentration of tumors treated with PEG-PCL/DOX or DOX and about 8-fold that of tumors treated with TAT-PEG-PCL/DOX (Figure 6d).

The antitumor mechanisms of the DOX-loaded nanoparticles were further analyzed by histological examination or immunohistochemistry. Hematoxylin/eosin (H&E) staining showed that tumors treated with PBS and TAT-PEG-PCL/DOX (Figure 7a–e) typically consisted of tightly packed tumor cells and some necrotic regions because of rapid tumor growth. However, extensive nuclear shrinkage and fragmentation were observed in the DOX- and ^{a}TAT-PEG-PCL/DOX-treated tumors. As shown by terminal deoxynucleotidyl transferase dUTP nick end labeling (TUNEL) staining (Figure 7a′–e′), tumors treated with DOX and ^{a}TAT-PEG-PCL/DOX had extensive regions of apoptotic cells; such apoptotic cells were much less present in the tumors treated with PEG-PCL/DOX, consistent with the H&E stain results. Statistical analysis of the apoptotic cells in three randomly selected tumor-section views showed that significantly ($p < 0.05$) more positive cells were found in the ^{a}TAT-PEG-PCL/DOX and DOX groups than in the PEG-PCL/DOX group (Figure S6 in the Supporting Information).

Loss of mouse body weight accompanied the treatment with DOX in this study (Figure S7 in the Supporting Information) but was not found in the ^{a}TAT-PEG-PCL/DOX group. Irreversible cardiotoxicity due to cardiomyocyte damage is a common side effect of DOX treatment.[34] To evaluate the myocardial damage induced by the DOX treatments, histological changes of cardiomyocytes were examined by light microscopy. As shown in Figure 7a″–e″, the PBS-, ^{a}TAT-PEG-PCL/DOX-, TAT-PEG-PCL/DOX-, and PEG-PCL/DOX-treated groups had compact cardiomyocytes lining up in order with clear structures similar to normal ones, but the DOX-treated group exhibited severe myocardial damage characterized by disorganized myofibrillar arrays.[35]

It was very surprising that ^{a}TAT had no effect on the PEG-PCL micelles' stealth property while greatly enhancing the accumulation in tumor tissues and therapeutic efficacy of DOX. The enhanced tumor accumulation by ^{a}TAT was possibly due to the enhanced cellular uptake, as active nanocarriers do.[36] Nanocarriers functionalized with ligands such as folic acid and integrin $\alpha v\beta 3$ have been found to enhance tumor accumulation compared with their unfunctionalized counterparts just because the ligands can bind their receptors on the tumor cells and enhance the cellular uptake of active nanoparticles via receptor-mediated endocytosis.[36] In this study, after ^{a}TAT-PEG-PCL micelles extravasated from the bloodstream into the tumor tissues, some ^{a}TAT was converted to native TAT at the acidic tumor interstitial pH,[23] leading to fast cellular uptake of the nanoparticles (as shown in Figure 3) and enhanced accumulation in tumor tissues. Thus, the resulting high tumoral drug concentration as well as the facilitated intracellular drug transport to the perinuclear region account for the better therapeutic efficacy of drug-loaded ^{a}TAT-PEG-PCL nanoparticles.

CONCLUSION

Using TAT as an example, we have demonstrated herein an efficient molecular modification approach that involves reversible blocking/activation of cationic CPPs. Amidization of the CPPs' lysine residues to succinyl amides can efficiently block their in vivo nonspecific interactions; once the amides are hydrolyzed in an acidic environment such as tumor extracellular fluids or endo/lysosomes, the CPPs' membrane-transduction and nuclear-localization activity are fully recovered. Compared with cationic charge-shielding approaches, the amidized CPPs are very stable and have completely inhibited nonspecific interactions in the blood compartment. Thus, coupled with tissue-specific targeting groups, this approach may greatly widen the door for in vivo applications of CPPs.

ASSOCIATED CONTENT

Supporting Information

Synthesis methods and NMR characterization data for the compounds, preparation of the micelles, sizes and morphologies of the micelles, cellular uptake, tumor inhibition rates, statistical analysis of apoptotic cells in tumor tissues, and changes in mice body weights during the treatment. This material is available free of charge via the Internet at http://pubs.acs.org.

AUTHOR INFORMATION

Corresponding Author

shenyq@zju.edu.cn

Author Contributions

‖E.J. and B.Z. contributed equally.

Notes

The authors declare no competing financial interest.

ACKNOWLEDGMENTS

This study was funded by the National Fund for Distinguished Young Scholars (50888001), the National Natural Science Foundation of China (21090352 and 20904046), the Program for Changjiang Scholars and Innovative Research Team, the University Fundamental Research Funds for the Central Universities of China (2012XZZX004), the Zhejiang Province Public Welfare Program (2011C21055), and the U.S. Department of Defense (BC083821).

REFERENCES

(1) Nakase, I.; Akita, H.; Kogure, K.; Graslund, A.; Langel, U.; Harashima, H.; Futaki, S. *Acc. Chem. Res.* **2012**, *45*, 1132. Patil, K. M.; Naik, R. J.; Fernandes, M.; Ganguli, M.; Kumar, V. A. *J. Am. Chem. Soc.* **2012**, *134*, 7196. Li, L.; Ge, J. Y.; Wu, H.; Xu, Q. H.; Yao, S. Q. *J. Am.*

Chem. Soc. **2012**, *134*, 12157. Marks, J. R.; Placone, J.; Hristova, K.; Wimley, W. C. *J. Am. Chem. Soc.* **2011**, *133*, 8995. Kumar, P.; Wu, H. Q.; McBride, J. L.; Jung, K. E.; Kim, M. H.; Davidson, B. L.; Lee, S. K.; Shankar, P.; Manjunath, N. *Nature* **2007**, *448*, 39. Joliot, A.; Prochiantz, A. *Nat. Cell Biol.* **2004**, *6*, 189. Covic, L.; Misra, M.; Badar, J.; Singh, C.; Kuliopulos, A. *Nat. Med.* **2002**, *8*, 1161. Wang, R. F.; Wang, H. Y. *Nat. Biotechnol.* **2002**, *20*, 149.

(2) Ruoslahti, E. *Adv. Mater.* **2012**, *24*, 3747.

(3) Vives, E.; Brodin, P.; Lebleu, B. *J. Biol. Chem.* **1997**, *272*, 16010.

(4) Lange, A.; Mills, R. E.; Lange, C. J.; Stewart, M.; Devine, S. E.; Corbett, A. H. *J. Biol. Chem.* **2007**, *282*, 5101.

(5) Lorberboum-Galski, H.; Rapoport, M. *Expert Opin. Drug Delivery* **2009**, *6*, 453. Yan, M.; Du, J. J.; Gu, Z.; Liang, M.; Hu, Y. F.; Zhang, W. J.; Priceman, S.; Wu, L. L.; Zhou, Z. H.; Liu, Z.; Segura, T.; Tang, Y.; Lu, Y. F. *Nat. Nanotechnol.* **2010**, *5*, 48.

(6) Shiraishi, T.; Nielsen, P. E. *Nat. Protoc.* **2006**, *1*, 633.

(7) Hoyer, J.; Neundorf, I. *Acc. Chem. Res.* **2012**, *45*, 1048.

(8) Chang, J.; Wang, H. J.; Zhang, S. N.; Liao, Z. Y.; Wang, C. Y.; Liu, Y.; Feng, S. Q.; Jiang, X. G. *Biomaterials* **2010**, *31*, 6589.

(9) Snyder, E. L.; Dowdy, S. F. *Pharm. Res.* **2004**, *21*, 389.

(10) Asoh, S.; Ohta, S. *Adv. Drug Delivery Rev.* **2008**, *60*, 499. Morris, M. C.; Depollier, J.; Mery, J.; Heitz, F.; Divita, G. *Nat. Biotechnol.* **2001**, *19*, 1173.

(11) Chou, L. Y. T.; Ming, K.; Chan, W. C. W. *Chem. Soc. Rev.* **2011**, *40*, 233. Lo, W.-L.; Chien, Y.; Chiou, G.-Y.; Tseng, L.-M.; Hsu, H.-S.; Chang, Y.-L.; Lu, K.-H.; Chien, C.-S.; Wang, M.-L.; Chen, Y.-W.; Huang, P.-I.; Hu, F.-W.; Yu, C.-C.; Chu, P.-Y.; Chiou, S.-H. *Biomaterials* **2012**, *33*, 3693.

(12) Endoh, T.; Ohtsuki, T. *Adv. Drug Delivery Rev.* **2009**, *61*, 704.

(13) Fonseca, S. B.; Pereira, M. P.; Kelley, S. O. *Adv. Drug Delivery Rev.* **2009**, *61*, 953. Margus, H.; Padari, K.; Pooga, M. *Mol. Ther.* **2012**, *20*, 525. Huang, J.; Lein, M.; Gunderson, C.; Holden, M. A. *J. Am. Chem. Soc.* **2011**, *133*, 15818.

(14) Schwarze, S. R.; Ho, A.; Vocero-Akbani, A.; Dowdy, S. F. *Science* **1999**, *285*, 1569.

(15) Sarko, D.; Beijer, B.; Boy, R. G.; Nothelfer, E. M.; Leotta, K.; Eisenhut, M.; Altmann, A.; Haberkorn, U.; Mier, W. *Mol. Pharmaceutics* **2010**, *7*, 2224.

(16) van Duijnhoven, S. M. J.; Robillard, M. S.; Nicolay, K.; Grull, H. *J. Nucl. Med.* **2011**, *52*, 279.

(17) Zhu, L.; Kate, P.; Torchilin, V. P. *ACS Nano* **2012**, *6*, 3491. Jiang, T.; Olson, E. S.; Nguyen, Q. T.; Roy, M.; Jennings, P. A.; Tsien, R. Y. *Proc. Natl. Acad. Sci. U.S.A.* **2004**, *101*, 17867.

(18) Sethuraman, V. A.; Bae, Y. H. *J. Controlled Release* **2007**, *118*, 216.

(19) Itaka, K.; Kataoka, K. *Curr. Gene Ther.* **2011**, *11*, 457.

(20) Lee, E. S.; Gao, Z. G.; Kim, D.; Park, K.; Kwon, I. C.; Bae, Y. H. *J. Controlled Release* **2008**, *129*, 228.

(21) Morris, M. C.; Chaloin, L.; Heitz, F.; Divita, G. In *Cell-Penetrating Peptides*; Langel, U., Ed.; CRC Press: Boca Raton, FL, 2002; p 93.

(22) Xu, P. S.; Van Kirk, E. A.; Zhan, Y. H.; Murdoch, W. J.; Radosz, M.; Shen, Y. Q. *Angew Chem., Int. Ed.* **2007**, *46*, 4999. Lee, Y.; Fukushima, S.; Bae, Y.; Hiki, S.; Ishii, T.; Kataoka, K. *J. Am. Chem. Soc.* **2007**, *129*, 5362. Du, J.-Z.; Sun, T.-M.; Song, W.-J.; Wu, J.; Wang, J. *Angew. Chem., Int. Ed.* **2010**, *49*, 3621.

(23) Helmlinger, G.; Yuan, F.; Dellian, M.; Jain, R. K. *Nat. Med.* **1997**, *3*, 177.

(24) Zhou, Z. X.; Shen, Y. Q.; Tang, J. B.; Fan, M. H.; Van Kirk, E. A.; Murdoch, W. J.; Radosz, M. *Adv. Funct. Mater.* **2009**, *19*, 3580.

(25) Hurd, C. D.; Prapas, A. G. *J. Org. Chem.* **1959**, *24*, 388.

(26) Shen, Y. Q.; Zhou, Z. X.; Sui, M. H.; Tang, J. B.; Xu, P. S.; Van Kirk, E. A.; Murdoch, W. J.; Fan, M. H.; Radosz, M. *Nanomedicine* **2010**, *5*, 1205.

(27) Kazuo, M. *Adv. Drug Delivery Rev.* **2011**, *63*, 161.

(28) Sawant, R.; Torchilin, V. *Mol. BioSyst.* **2010**, *6*, 628. Liu, J.-N.; Bu, W.; Pan, L.-M.; Zhang, S.; Chen, F.; Zhou, L.; Zhao, K.-l.; Peng, W.; Shi, J. *Biomaterials* **2012**, *33*, 7282.

(29) Savic, R.; Luo, L. B.; Eisenberg, A.; Maysinger, D. *Science* **2003**, *300*, 615. Shuai, X.; Ai, H.; Nasongkla, N.; Kim, S.; Gao, J. *J. Controlled Release* **2004**, *98*, 415.

(30) Panté, N.; Kann, M. *Mol. Biol. Cell* **2002**, *13*, 425.

(31) Pan, L.; He, Q.; Liu, J.; Chen, Y.; Ma, M.; Zhang, L.; Shi, J. *J. Am. Chem. Soc.* **2012**, *134*, 5722.

(32) Szakacs, G.; Paterson, J. K.; Ludwig, J. A.; Booth-Genthe, C.; Gottesman, M. M. *Nat. Rev. Drug Discovery* **2006**, *5*, 219.

(33) Lu, Y. J.; Sega, E.; Leamon, C. P.; Low, P. S. *Adv. Drug Delivery Rev.* **2004**, *56*, 1161.

(34) Minotti, G.; Menna, P.; Salvatorelli, E.; Cairo, G.; Gianni, L. *Pharmacol. Rev.* **2004**, *56*, 185.

(35) Xu, Y.; Liu, Z.; Sun, J.; Pan, Q.; Sun, F.; Yan, Z.; Hu, X. *PLoS One* **2011**, *6*, No. e28335.

(36) Xiong, X.-B.; Uludağ, H.; Lavasanifar, A. *Biomaterials* **2010**, *31*, 5886.